INTERNATIONAL JOURNAL FOR NUMERICAL AND ANALYTICAL METHODS IN GEOMECHANICS, VOL. 22, 175–196 (1998)

PROPAGATION OF A SHEAR CRACK IN A COMPRESSED PLANE WITH A CIRCULAR HOLE

A. N. GALYBIN

Geomechanics Group, Dept. of Civil Engng. The University of Western Australia, Nedlands, WA 6907, Australia

SUMMARY

The problem of the equilibrium of a plane with a circular hole and a shear crack is considered to model failure of an excavation (borehole or circular opening) in rocks weakened by discontinuities (planes of weakness). It is assumed that sliding occurs in a part of the plane of weakness when the Mohr–Coulomb friction criterion is satisfied due to the stress redistribution caused by the excavation. The method of singular integral equations is employed to solve the boundary value problem. Geomechanical problems concerning borehole breakout and rockburst caused by fault-opening interaction are discussed. © 1998 John Wiley & Sons, Ltd.

Int. J. Numer. Anal. Meth. Geomech., vol. 22, 175–196 (1998)

Key words: shear crack; singular integral equation; excavation; discontinuities

1. INTRODUCTION

Plane elastic problems for a body weakened by holes and cracks have continuously been considered as models of fracture processes in materials, constructions, mechanisms and rock masses. The first results[1] were obtained by using the method of conformal mapping for solving the problem of a plane with a circular hole and radial cracks. Then the method of singular integral equations was applied for solving similar problems[2] and, later, different numerical methods were applied for various arrangements of crack and holes and boundary conditions (see References 3 and 4 for details).

In the present paper the method of singular integral equations in the form proposed by Savruk[5] is used for solving the problem for an elastic isotropic plane weakened by a circular hole and a shear crack. The main difference of the present mathematical formulation from the previous ones is that the position of the shear crack is defined in the process of solving by assuming boundedness of stresses at both crack ends. This fact and also a number of involved parameters require applying fast methods of calculating the stress intensity factors at the crack tips. Using the Gauss quadrature formulae for evaluation of singular integrals[6] allowed to obtain solutions and perform the parametric analysis on the basis of capabilities offered by the package MATHCAD5+.

* Correspondence to: A. N. Galybin, Geomechanics Group, Department of Civil Engineering, The University of Western Australia, Nedlands, WA 6907, Australia

CCC 0363–9061/98/030175–22$17.50

Received 28 May 1996
Revised 20 May 1997

The considered mathematical problem arises from one of the main problems in mining and petroleum engineering: instability of underground openings and boreholes in rocks weakened by discontinuities. One of the mechanisms of failure of rockmass near openings is sliding along discontinuities (planes of weakness) such as joints or geological faults. Other possible mechanisms of failure (e.g. tensile failure, bending of layers, etc.) are out of the scope of this study.

Sliding can mainly be initiated due to the influence of the opening. The additional (opening-induced) stresses are distributed non-uniformly, hence sliding would start to propagate over a part of the plane of weakness where shear stresses exceed the shear resistance. To estimate the length of a sliding zone, one can use elastic solutions. However, only a lower estimation of the length can be obtained by this manner, because once the sliding zone has appeared it can, in principle, propagate further.

It is emphasized in a well-known textbook[7] (p. 189) that in some excavation design problems "an elastic analysis . . . provides a basis for judgement of engineering significance of a discontinuity". This statement has been illustrated there through convincing examples for a circular opening located near a discontinuity whose strength is defined by the friction angle only. More rigorous analysis of the elastic solution for the circular opening is conducted in the present paper where both cohesion and friction are considered. Furthermore, it takes into account the effect of internal pressure simulating the action of support in excavations or mud pressure in boreholes.

The results of this analysis are used further to investigate the propagation of sliding along the discontinuity. Namely, the initial length of the sliding zone is calculated from the elastic solution and then used as an initial guess in an iteration process of determining the final length of the sliding zone. For this purpose sliding is modelled as a pure shear crack whose balanced length is determined by equating the mode II stress intensity factor to the corresponding fracture toughness. It should be noted that knowing the actual size of the sliding zone is important, since it determines the amount of released seismic energy. Hence the dimension of the sliding zone can serve as an estimation of the energy emission during a possible rockburst.

In the present paper a possibility of rockbursts induced by an instantaneous slip over a discontinuity is considered together with the mechanically similar process of an initial stage of breakout formation near boreholes in jointed rocks. The only difference is that in the latter case the presence of joints makes the deformation (not only strength) characteristics of rocks to be anisotropic. However, the joint-induced anisotropy depends on the relative distance between joints with respect to the diameter of the opening.[8] For the case of relatively small openings (like boreholes), the influence of deformation anisotropy on the stress field can often be neglected, since essential modification of deformation characteristics can be expected after sliding along a certain number of joints.

Mathematical aspects in both these cases are similar, hence the mathematical problem is considered separately at first. Then applications are considered. Finally, a discussion of applicability of approximate solutions which have been used for solving similar problems[9] is provided.

2. MATHEMATICAL MODEL

2.1. Statement of the problem

The equilibrium of a plane with a circular hole of radius R and a shear crack of length l is considered. The plane is subjected to the plane-strain conditions under biaxial compression at

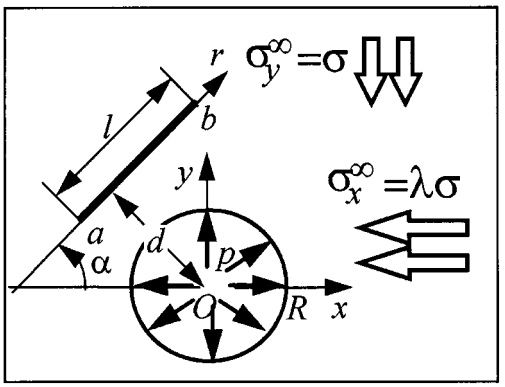

Figure 1. Hole and shear crack in plane

infinity and internal pressure acting in the hole (Figure 1). The medium is assumed to be elastic and isotropic.

Let the Cartesian coordinate system Oxy be coaxial with the directions of the remote principal stresses, and the origin be placed at the centre of the hole. By introducing a complex variable $z = x + \mathrm{i}y$ one can represent the contour of the hole as $\gamma = \{z : |z| = R\}$. Let the crack be inclined at an angle α with respect to the positive x-direction and located at a distance d from the centre of the hole. Then the contour of the crack can be written in the form $\mathbf{L} = \{z : z = (r + \mathrm{i}d)\exp(\mathrm{i}\alpha), a \leqslant r \leqslant b, b - a = l\}$.

The principal stresses at infinity are denoted by $\sigma_x^\infty = \lambda\sigma$, $\sigma_y^\infty = \sigma$ and the internal pressure acting in the hole by p. It is assumed that sliding along the crack is governed by the Mohr–Coulomb criterion. Then the boundary conditions of the problem can be written in the form

$$\begin{aligned} &z \in L: |\tau_a| + \sigma_\mathrm{n} \tan\rho = \tau_\mathrm{c}, \quad \sigma_\mathrm{n} < 0, \\ &[\sigma_\mathrm{n}] = [\tau_\alpha] = 0, \qquad [u_\mathrm{n}] = 0 \\ &z \in \gamma: \quad \sigma_r = p, \qquad \tau_{r\theta} = 0 \\ &z \to \infty: \quad \sigma_x \to \lambda\sigma, \quad \sigma_y \to \sigma, \quad \tau_{xy} \to 0 \end{aligned} \tag{1}$$

Here τ_α, σ_n are shear and normal stresses at the crack, respectively, ρ, τ_c are the friction angle and the cohesion along the crack respectively, and u_n is the normal displacement at the crack. Square brackets denote a jump of a value at the crack line.

Introducing an unknown jump of tangential displacements, $[u_\alpha]$, over the crack contour one can express the complex potentials $\Phi(z)$ and $\Psi(z)$ describing the stress state of the plane in the form[5,10]

$$\Phi(z) = \Phi_1(z) + \Phi_2(z), \qquad \Psi(z) = \Psi_1(z) + \Psi_2(z) \tag{2}$$

$$\Phi_1(z) = -\frac{\sigma}{2} + \frac{\sigma(1-\lambda)}{4}\left(1 - \frac{2}{z^2}\right), \qquad \Psi_1(z) = \frac{p-\sigma}{z^2} - \frac{\sigma(1-\lambda)}{2}\left(1 - \frac{2}{z^2} + \frac{3}{z^4}\right) \tag{3}$$

$$\Phi_2(z) = \frac{1}{2\pi i}\int_\alpha^b \left[\frac{e^{i\alpha}}{t(r)-z} + \Phi^*(z,t(r))\right]\mu(t)dr,$$

$$\Psi_2(z) = \frac{1}{2\pi i}\int_a^b \left[\frac{e^{-i\alpha}}{z-t(r)} - \frac{\overline{t(r)}e^{i\alpha}}{(t(r)-z)^2} + \Psi^*(z,t(r))\right]\mu(t)\,dr \tag{4}$$

$$\Phi^*(z,t) = \frac{e^{i\alpha}}{z(z\bar{t}-1)} - \frac{(1-t\bar{t})e^{-i\alpha}}{\bar{t}(z\bar{t}-1)^2} + \frac{e^{i\alpha}}{z}$$

$$\Psi^*(z,t) = \left[\frac{1}{z(1-z\bar{t})} + \frac{(1-t\bar{t})(1-3z\bar{t})}{z^2\bar{t}(z\bar{t}-1)^3} - \frac{1}{z}\right]e^{-i\alpha} + \left[\frac{3z\bar{t}-2}{z^3(z\bar{t}-1)^2} + \frac{1}{z^2 t} + \frac{2}{z^3}\right]e^{i\alpha}$$

$$t = t(r) = (r + id)\exp(i\alpha)$$

Here z is the complex coordinate of a point in the plane, $\mu(t) = \{G/[2(1-\nu]\}(d/dt)[u_\alpha(t)]$ is the real function proportional to the derivative of the jump in tangentinal displacements; G and ν are the shear modulus and Poisson's ratio, respectively.

The potentials denoted by subscript 1 are related to the stresses in the biaxially loaded plane with the pressurized hole, but without the crack (Problem 1). The potentials with subscript 2 correspond to the stress state in the plane containing the hole, which will be induced by relative shearing the crack faces while the loads at infinity and on the hole contour are absent (Problem 2). The sum of these potentials satisfies both the boundary conditions at infinity and on the hole contour for any arbitrary given function, $\mu(\eta)$. In order to satisfy the boundary conditions at the crack, the unknown function $\mu(\eta)$ should be determined from the following singular integral equation whose kernel does not depend on the angle α:

$$\frac{1}{2\pi}\int_{-1}^{1}\left[\frac{2}{\eta-\xi} + G(\eta,\xi)\right]\mu(\eta)\,d\eta = \chi(\tau_c - F(\xi)), \quad |\xi| < 1 \tag{5}$$

where

$$G(\eta,\xi) = \mathrm{Re}[\Omega(z(\eta),z(\xi))] + \tan(\chi\rho)\,\mathrm{Im}[\Omega(z(\eta),z(\xi))]$$

$$F(\xi) = \mathrm{Re}[\Omega_1(z(\xi))] + \tan(\chi\rho)\,\mathrm{Im}[\Omega_1(z(\xi))]$$

$$z(\xi) = (0{\cdot}5l\xi + c + id)e^{i\alpha}, \quad l = b-a, \quad c = (b+a)/2, \quad \chi = \pm 1$$

$$\Omega(t,z) = -\frac{il}{2}[\Phi^*(t,z) - \overline{\Phi^*(t,z)} + e^{2i\alpha}(\bar{z}\Phi^{*\prime}(t,z) + \Psi^*(t,z))]$$

$$\Omega_1(z) = \Phi_1(z) + \overline{\Phi_1(z)} + e^{2i\alpha}(\bar{z}\Phi_1'(z) + \Psi_1(z))$$

In equation (5) the symbol for the absolute value of shear stresses in the Mohr–Coulomb criterion has been removed as follows. Let τ_α^1 be the shear stress from Problem 1 and let it be sufficient to induce sliding over the crack ($\tau_\alpha^1 + \sigma_n^1\tan\rho > \tau_c, \sigma_n^1 < 0$). Then the diretction of sliding is predetermined by the sign of the shear stresses $\chi = \mathrm{sgn}[\max(\tau_\alpha^1)]$. This means that the compensating shear stress from Problem 2, τ_α^2, has to have the opposite sign to eliminate the excess in the left-hand side of the Mohr–Coulomb criterion. However, its magnitude over the crack line cannot exceed the maximum magnitude of τ_α^1, hence the total shear stresses would have the same sign as τ_α^1, hence $\chi = \mathrm{sgn}(\tau_\alpha^1 + \tau_\alpha^2)$.

By replacing the stress components in the Mohr–Coulomb criterion with the sum of the corresponding components in the Problems 1, 2 and multiplying by χ, one has

$$\tau_\alpha^2 + \sigma_n^2 \tan(\chi\rho) = \chi(\tau_c - |\tau_\alpha^1| - \sigma_n^1 \tan\rho) = \chi(\tau_c - F) \tag{6}$$

Then equation (5) follows from equation (6) by expressing the stress components from the complex potentials (4) by using the Kolosov formulae.[10]

The solution of equation (5) has to satisfy the condition of the single-valuedness of the displacements

$$\int_{\mathbf{L}} \mu(t)\,\mathrm{d}t = u_0 \tag{7}$$

In the general case, the shear crack may either intersect the boundary of the hole or may be located adjacent to it. Both these cases are considered here. For the case of non-intersection, equation (5) belongs to the type of singular integral equations which always have unbounded solution (satisfying condition (7), when $u_0 = 0$) at the ends. For edge cracks the condition of the single-valuedness of displacements must hold over the total contour $\mathbf{L} \cup \gamma$, which means that the value u_0 is not equal to zero. In this case the function $G(\eta, \xi)$ in the kernel of equation (5) contains a fixed singularity at the point of intersection, which makes solving the equation more complicated.

Solvability of equations of this kind has been examined by Duduchava.[11] In particular, this kind of equation has been shown to permit a unique solution bounded at the crack mouth (the point where the crack intersects the hole) and unbounded at the other end. On the other hand, an unbounded solution at the crack mouth is also available for an equation of this kind. The singularity at this point is less than the square-root singularity at the crack end and depends on the angle between the crack and the free surface.[12] Moreover, the order of singularity may depend on applied load.[13] However, in many cases the full account of weak singularities does not strongly affect the result. Hence, a numerical solution can be derived by the method proposed by Savruk[5] (see details in the next subsection). One can compare, for instance, the results of numerical calculations[5] for the stress intensity factors for a half-plane with an inclined edge crack with exact calculations.[14] In the present paper the approximate method[5] is used.

Equation (5) and condition (7) represent the boundary value problem (1) of the elastic equilibrium of a plane with a hole and a shear crack of an arbitrary disposition. The mathematical solution of this problem exists independently of geometry and magnitudes of applied stresses. However, the solution of this mathematical problem will be used further for analysis of sliding propagation over a plane of weakness in a rock-mass with a circular opening. Therefore, the following restrictions reflecting a mechanical situation should be taken into account: (a) there is no sliding in the intact rock-mass; (b) sliding over a part of the plane of weakness has to start if and only if the effective shear stresses in Problem 1 exceed the shear resistance; and (c) the propagation of sliding over the plane of weakness is governed by a criterion of fracture (for instance, $K_{\mathrm{II}} = K_{\mathrm{IIc}}$).

The first restriction can easily be written as an inequality. By calculating the shear and normal stresses in Problem 1 in the direction parallel to the plane of weakness one obtains

$$\left(\lambda + \frac{\tau_c}{\sigma}\cot\rho\right)\tan^2\alpha - \cot\rho\,|(1-\lambda)\tan\alpha| + \left(1 + \frac{\tau_c}{\sigma}\cot\rho\right) > 0 \tag{8}$$

The second restriction means that before solving equation (5) it is necessary to set an initial approximation for the co-ordinates of the ends, a_0, b_0, of the shear crack. These values can be obtained from the elastic solution given by the potentials (3) in the following manner. The function $F(\xi)$ in the right-hand side of equation (5) may be represented as a function of seven variables

$$F(r, d, \alpha, \lambda, \sigma, p, \rho) = |\tau_\alpha^1(z(r, d, \alpha), \lambda, \sigma, p)| + \sigma_n^1(z(r, d, \alpha), \lambda, \sigma, p)\tan\rho \tag{9}$$

The first three variables, r, d, α, characterize the position of the plane of weakness where the left-hand side of the Mohr–Coulomb criterion is calculated. The other variables specify the load λ, σ, p, and friction angle, ρ. If the inclination of the shear crack, α, its distance from the hole center, d, and the parameters λ, σ, p, ρ are fixed, one can consider the function F as a function of the only variable r. To determine the initial positions of the crack ends a_0, b_0, consider the equation

$$F(r, d, \alpha, \lambda, \sigma, p, \rho) = \tau_c \tag{10}$$

which has a set of roots, r^*. The required roots $r^* = a_0$, $r^* = b_0$ should be chosen as the nearest roots to the point of supremum, $r^{\sup}$, of function F so that $a_0 < r^{\sup} < b_0$. Note that the values of a_0, b_0 obtained will, obviously, be dependent on the seven parameters $a_0 = a_0(d, \alpha, \lambda, \sigma, p, \rho, \tau_c)$, $b_0 = b_0(d, \alpha, \lambda, \sigma, p, \rho, \tau_c)$.

The last restriction (c) determines the final position (and the length) of the crack that started to propagate over the plane of weakness. Since sliding is assumed not to induce any crack opening, the condition of the shear crack growth can be determined by the mode II stress intensity factor (SIF), K_{II}, only. The magnitudes of SIFs at the left, K_{II}^l, and the right, K_{II}^r, ends are different and depend on the position of the crack (parameters a, b, d, α) and the parameters of load and strength. In order to determine the maximum size of the shear crack one can assume the following crack growth for the case when the crack does not intersect the hole

$$K_{II}^{l,r}(a, b, d, \alpha, \lambda, \sigma, p, \rho, \tau_c) = 0 \tag{11}$$

If the crack intersects the hole condition (11) is only assumed for the remote end, since the SIF for another end is zero.

Condition (11) constitutes a system of two equations for determination of a, b while the other parameters are fixed. Then similarly to the initial values a_0, b_0, one can represent the final values a and b as functions of seven variables $a = a(d, \alpha, \lambda, \sigma, p, \rho, \tau_c)$, $b = b(d, \alpha, \lambda, \sigma, p, \rho, \tau_c)$. The final and initial values have to satisfy the following obvious inequality

$$a \leqslant a_0 < b_0 \leqslant b \tag{12}$$

It should be noted that any other values of a, b obtained from the general criterion $K_{II} = K_{IIc}$ will be situated between the corresponding initial and final values obtained from criterion (11). This means that the proposed approach gives both the initial and final positions of the crack independently of the mode II fracture toughness, K_{IIc}.

Finally, the mathematical problem considered includes

(i) singular integral equation (5);
(ii) the single-valuedness condition of displacements (7);

(iii) restriction (8); and
(iv) equations (9)–(12) for determining the position of the crack ends.

2.2. Numerical method

Since the kernel of singular integral equation (5) contains a regular part of a non-degenerate type, its solution cannot be obtained analytically, hence a numerical method should be applied. Methods based on the Gauss–Chebyshev numerical integration rule[6] for a singular operator seem to be the most convenient especially for calculating the stress intensity factors. Having high accuracy, they do not require a large number of calculations. Here a variant of the direct method[5] will be mainly used for both the internal and edge cracks. The results presented by Savruk[5] show that 10–20 nodes are sufficient to calculate the SIFs in many particular cases including edge cracks. Another variant of this method,[15] which is based on applying the Gauss–Chebyshev integration to regularised equations, will also be used for the sake of comparison.

The direct application of Gauss–Chebyshev numerical integration rule to equation (5) and condition (7) reduces the boundary value problem to the following system of algebraic equations

$$\frac{\chi}{2N}\sum_{j=1}^{N}\left[\frac{2}{\eta_j-\xi_m}+G(\eta_j,\xi_m)\right]\mu_{0j}=\tau_c-F(\xi_m),\quad m=1,\ldots,N-1 \tag{13}$$

$$\sum_{j=1}^{N}\mu_j=0 \tag{14}$$

Here

$$\eta_j=\cos\left(\frac{2j-1}{2N}\pi\right),\qquad \xi_m=\cos\left(\frac{m\pi}{N}\right),\qquad \mu_{0j}=\mu(\eta_j)\sqrt{1-\eta_j^2}$$

The normalized stress intensity factors can be calculated by using formulae

$$K_{\mathrm{II}}^{\mathrm{l,r}}=\pm\mu_0(\pm 1),\quad \mu_0(1)=\frac{-1}{N}\sum_{j=1}^{N}(-1)^j\mu_{0j}\cot\left(\frac{2j-1}{4N}\pi\right),$$

$$\mu_0(-1)=\frac{1}{N}\sum_{j=1}^{N}(-1)^{j+N}\mu_{0j}\tan\left(\frac{2j-1}{4N}\pi\right) \tag{15}$$

The system of algebraic equations (13) and (14) is valid for internal cracks only. For the case of intersection, equation (14) has to be corrected since the jump of tangential displacements is not equal to zero at the mouth of the shear crack. Following Savruk[5] it is assumed that the density of the jump is bounded at the point of intersection. It gives $\mu_0(1)=0$, if the right end of the crack belongs to hole contour or $\mu_0(-1)=0$ otherwise. Hence (14) is replaced by

$$\sum_{j=1}^{N}(-1)^j\mu_{0j}\cot\left(\frac{2j-1}{4N}\pi\right)=0\quad\text{or}\quad\sum_{j=1}^{N}(-1)^{j+N}\mu_{0j}\tan\left(\frac{2j-1}{4N}\pi\right)=0 \tag{16}$$

Using (16) means that the density of the jump of displacements is assumed to be zero at the crack mouth, which is a simplification of the numerical procedure. A more accurate approach based on accounting for weak singularities at the crack mouth has been developed by Theocaris and Ioakimidis.[16] However, using the accepted simplification one may expect to obtain accurate results because of boundedness of the solution at the crack mouth.

The boundedness follows from the analysis of the corresponding Winner–Hopf problem[17] for the limiting case $l \ll R$ (edge crack in a half-plane). In this case the kernel of equation (5) does not depend on the crack length and is the kernel of the Mellin convolution type. Hence the application of the Mellin transform[12] to equation (5) will give the Winner–Hopf problem similar to that obtained by Cherepanov[17] by applying the Mellin transform directly to the general equations of elasticity. This problem can be written in the form

$$V^-(s) = G(s)(V^+(s) + F^-(s)) \tag{17}$$

where

$$G(s) = \tan(\pi s)\,[G_1(s)]^{-1}$$

$$G_1(s) = 1 + \cos(2s\alpha)\{2s^2\cos^2\alpha - 1 + s\tan(2s\alpha)[2(s-1)\tan\rho\cos^2\alpha - \sin(2\alpha)]\}\cos^{-2}(\pi s)$$

$$V^-(s) = \int_0^1 \mu(t)t^s\,\mathrm{d}t, \quad V^+(s) = \int_1^\infty (|\tau_\alpha(t)| + \sigma_n(t)\tan(\chi\rho))t^s\,\mathrm{d}t, \quad F^-(s) = \int_0^1 \chi(\tau_c - F(t))t^s\,\mathrm{d}t$$

For all angles $0 < \alpha < \pi/2$ and values of ρ, the coefficient $G(s)$ has no poles in the strip $-1 \leqslant \mathrm{Re}(s) < 0$. After applying the inverse Mellin transform to equation (17), the behaviour of the function $\mu(t)$ when $t \to 0$ will be of order $t^{-1-\delta}$, where δ is the nearest to the origin, $s = 0$, residual of the function $G(s)$ lying in the left half-plane $\mathrm{Re}(s) < 0$. Since $\delta \leqslant -1$, $\mu(t)$ is bounded at the crack mouth $t = 0$. Accounting for the regular terms in the kernel of (5) for an arbitrary l cannot change the behaviour of the solution, so the boundedness of the solution is also valid at the point of intersection of the shear crack and the hole.

Equivalence of the direct numerical method and the method based on preliminary regularization with further application of the quadrature formulae has been proved by Ioakimidis and Theocaris[15] for the case of the function $G(\eta, \xi)$ in the kernel of equation (5) bounded and regular for $-1 \leqslant \xi, \eta \leqslant 1$ (i.e. satisfying to the Holder condition with respect to both variables). Some modification will be required when the function $G(\eta, \xi)$ has singularities at boundary points $\xi = \eta = \pm 1$. This case will not be considered here.

The regularization of equation (5) gives

$$\mu(t) = \mu^0(t) + \int_{+1}^1 G_1(y,t)u(y)\,\mathrm{d}y + \frac{C}{\pi\sqrt{1-t^2}} \tag{18}$$

where

$$\mu^0(t) = \frac{-\chi}{\pi\sqrt{1-t^2}}\int_{-1}^1 \frac{\sqrt{1-x^2}}{x-t}[\tau_c - F(x)]\,\mathrm{d}x,$$

$$G_1(y,t) = \frac{1}{2\pi^2\sqrt{1-t^2}}\int_{-1}^1 \frac{\sqrt{1-x^2}}{x-t}G(y,x)\,\mathrm{d}x$$

Due to condition (14) the term containing the constant C vanishes.

Applying the Gauss–Chebyshev rule to equation (18) leads to a system of linear algebraic equations which may be presented in the form convenient for iterative calculations

$$\mu_{0j}^n = \mu_{0j}^0 + \sum_{k=1}^N B_{j,k}\mu_{0k}^{n-1}, \quad j = 1, \ldots, N-1 \tag{19}$$

where

$$B_{j,k} = \frac{1}{N^2} \sum_{m=1}^{N-1} \frac{w_m G(y_k, x_m)}{x_m - t_j}, \quad w_m = \sin^2\left(\frac{m\pi}{N}\right)$$

The first terms in equations (18) and (19) refer to tractions acting on the crack due to the stresses induced by the hole, while the second terms corresponds to interaction between the crack and the hole. In order to compare their contributions the above iterative method will be further applied for the case of non-intersection of the crack and the hole.

To satisfy equation (11) it is necessary to calculate SIFs for different positions of the crack, which gives a system of two non-linear equations for determining the coordinates of the crack ends. This problem is also solved numerically by using the Newton iterative method (provided by MATHCAD 5+) with initial value of a_0, b_0 defined from equation (10).

3. INITIATION OF SLIDING

The elastic stress state created by the circular opening and prior to any sliding along the discontinuity (plane of weakness in rockmass) is analysed in this section (Problem 1). Following the analysis presented by Brady and Brown[7] it is assumed that the presence of the discontinuity does not affect the deformation characteristics of the rockmass. As has been mentioned above, this analysis is also necessary to determine the initial positions and lengths of the sliding zones.

3.1. Ranges of variation of involved parameters

The stress state in Problem 1 depends on the following parameters: d, α, r, R, λ, σ, p. In order to find the initial positions of the sliding zones (the roots of equation (10): $r^* = a_0$, $r^* = b_0$; see Section 2) strength parameters, ρ, τ_c, should be incorporated.

The number of parameters involved can be reduced by introducing the corresponding dimensionless parameters as follows. Parameters of the units of length, d, r, a_0, b_0, are normalized with respect to the hole radius (which is equivalent to setting $R = 1$). Parameters of the units of stresses, p, τ_c, all stress components, and correspondingly the effective shear stresses, $F = |\tau_\alpha| + \sigma_n \tan\rho$, are normalized with respect to the vertical *in situ* stress acting at the considered depth, so $\sigma = 1$. The other parameters α, λ, ρ are already dimensionless.

Since the decrease in stresses produced by the hole is inversely proportional to the second power of distance from the hole centre, the working range for parameter d is assumed to be within $0 \leqslant d \leqslant 3$. Due to symmetry the range for the angle α is $0^\circ \leqslant \alpha < 90^\circ$.

The *in situ* stress ratio, λ, may, in principle, vary in a wide range depending on the depth and the region.[18] Here λ is assumed to lie between 1/3 and 3, in which case the condition of non-appearance of tensile stresses near the hole will be satisfied.

Internal pressure caused by borehole fluid or by the support in the excavation cannot usually exceed the vertical *in situ* stress, so in this study the value of p is assumed to be between $p = 0$, no internal pressure (e.g. a dry borehole) and $p = 0{\cdot}6$, a value corresponding approximately to the mud pressure in drilling operations ($p = 0{\cdot}4$ corresponds to the ratio of the density of water to the average density of rocks).

Since the friction angle and the cohesion along the discontinuity are usually much lower than those associated with the intact rock,[19] the range for the friction angle is assumed to be $0^\circ < \rho < 30^\circ$. The normalized parameter, τ_c, can vary over a wide range $\tau_c^{\min} \leqslant \tau_c \leqslant \tau_c^{\max}$. Here

the minimum value, τ_c^{min}, can be determined from inequality (8). The maximum value τ_c^{max} is chosen to be equal to the maximum effective shear stresses (supremum of the function F) acting over the discontinuity when other parameters d, α, λ, p, ρ are fixed.

3.2. *Admissible orientations of discontinuities*

The stress state in an intact rock mass is defined by the complex potentials (3) where $z \to \infty$ and depends on the principal *in situ* stresses (defined by only one parameter, λ, after normalization). For a homogeneous rock *in situ* stresses are not supposed to exceed the rock strength. Since discontinuites in the form of planes of weakness are assumed to be stable before excavating, the effective shear stresses, $|\tau_\alpha| + \sigma_n \tan\rho$, acting over these planes cannot exceed the resistance to shear rupture.

Let us consider probable orientations of the discontinuity with respect to the principal *in situ* stresses. As mentioned above inequality (8) must be satisfied to provide equilibrium of the discontinuity in an intact rockmass. If the cohesion is much less than the vertical stress at infinity, $\tau_c \ll 1$, which is the case in most real situations, expression (8) assumes the simple form

$$\lambda \tan^2\alpha - \cot\rho|(\lambda - 1)\tan\alpha| + 1 > 0 \tag{20}$$

This condition is not satisfied for some angles α depending on the friction angle ρ, and the ratio of the principal stresses λ. The ranges of admissible angles α (i.e. angles satisfying (20)) are shown in Figure 2 for different combinations of the parameters λ, ρ. The curves show regions of admissible (above the curves) and non-admissible (below the curves) angles α for different values of λ. As is obvious from Figure 2, in the case of high non-uniformity of the *in situ* stresses and low resistance to shear rupture, the range of possible angles of the discontinuity inclination is small. For instance, for $\lambda = 2$ and $\rho = 10^\circ$, the angle α should not be between 10° and 70°.

When cohesion increases the range of admissible angles becomes wider, Figure 3. As in Figure 2, the curves show regions of admissible (above the curves) and non-admissble (below the curves) angles α for different values of τ_c. One can see that any angle α is admissible for the above example of $\lambda = 2$ and $\rho = 10^\circ$, if $\tau_c > 0{\cdot}25$.

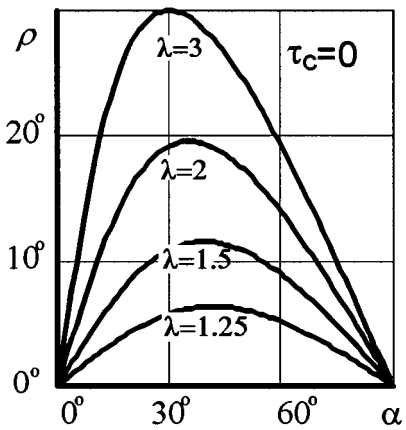

Figure 2. Discontinuity orientation, α, versus the friction angle ρ and the *in situ* stress ratio, λ

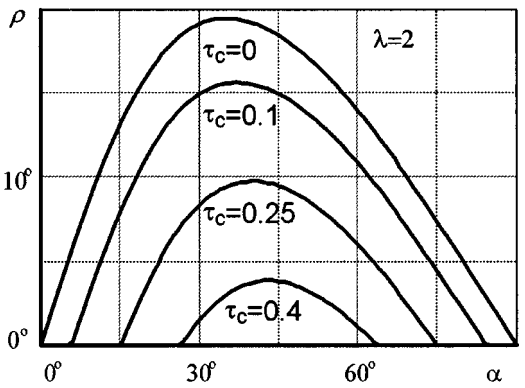

Figure 3. Discontinuity orientation, α, versus the friction angle, ρ, and the normalized cohesion, τ_c

3.3. *Distribution of effective shear stresses over the discontinuity*

When the hole is excavated the effective shear stresses given by expression (9), may exceed the resistane to shear rupture of the discontinuity (cohesion in the case considered). Then sliding will start to propagate over the discontinuity until a new state of equilibrium is reached. Analysis of the sliding propagation will be given in the next section. Here an initial analysis of the stress state preceding sliding is considered.

The maximum values of the effectve shear stresses $F_{\max} = F_{\max}(d, \alpha, \lambda, p, \rho)$ obtained as the maximum of the right-hand side of expression (9) with respect to the first variable were calculated by using complex potentials (3) and the Kolosov formulae. They are plotted in a dimensionless form in Figures 4 and 5. Figure 4 illustrates the case of hydrostatic *in situ* stress $\lambda = 1$ (in this case $F_{\max}$ does not depend on the angle α), whereas Figure 5 presents non-hydrostatic cases.

As one can see from Figure 4, the function $F_{\max}(d, \alpha, \lambda, p, \rho)$ always has a maximum (with respect to parameter d) at the hole boundary ($0 < d < 1$). This is also valid for non-hydrostatic *in situ* stresses (Figure 5). Increasing both the friction angle and the internal pressure results in decreasing $F_{\max}$ (Figures 4 and 5). The *in situ* stress ratio λ sufficiently affects the effective shear stresses. As one can see from Figure 5, the maximum values of the function $F_{\max}$ differ by a factor of approximately two for $\lambda = 1/2$ and $\lambda = 2$.

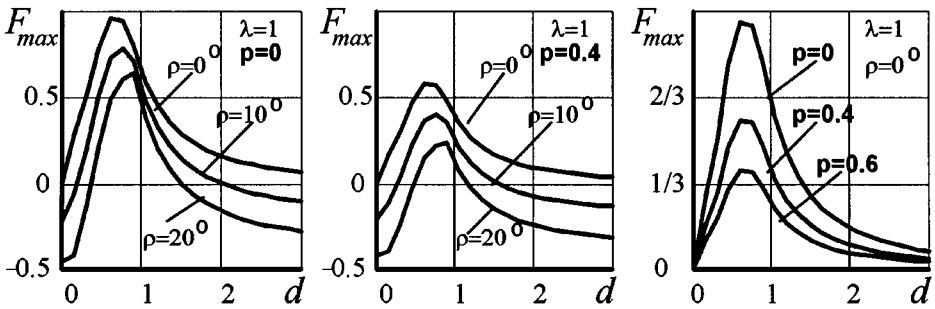

Figure 4. Maximum effective shear stresses $F_{\max}$.. Hydrodstatic *in situ* stresses

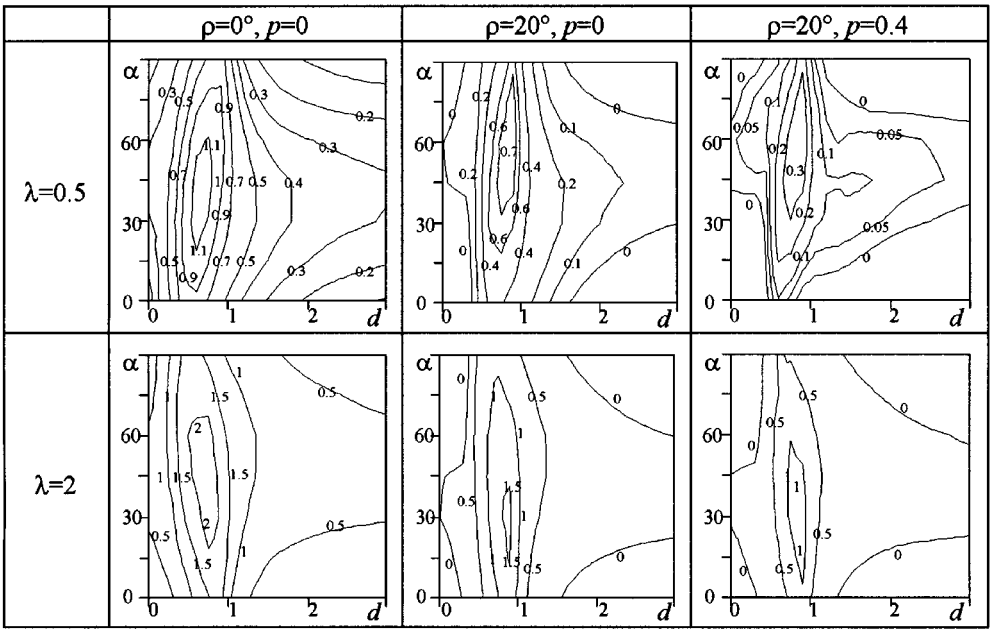

Figure 5. Maximum effective shear stresses $F_{\max.}$. Influence of the *in situ* stress ratio, λ, the friction angle, ρ, and the normalized internal pressure, p

3.4. *Initial sliding zones*

Results presented in Figures 4 and 5 show that it is possible to define a set of parameters λ, p, ρ, τ_c such that $F_{\max}(d, \alpha, \lambda, p, \rho) > \tau_c$ for any given position, d, α, of the discontinuity. Then equation (10) will have roots with respect to variable r in the vicinity of the point of supremum of function $F(r, d, \alpha, \lambda, p, \rho)$, see Section 2. These roots, a_0, b_0, determine the initial position of the sliding zones depending on the other parameters involved. It is convenient to use the complex plane $z = x + iy$ to present all available solutions of equation (10) as a boundary of a 2-D domain which will be further named as the *initial sliding zone*. Examples of initial sliding zones are presented on Figures 6 and 7 for different parameters α, λ, p, ρ, τ_c (numbers near the lines refer to the value of τ_c). The reduction of the initial sliding zones due to increase in internal pressure and/or friction angle is shown in Figure 6 for the hydrostatic stress state ($\lambda = 1$). The influence of the *in situ* stress ratio λ on shapes of the sliding zones is shown in Figure 7 for $\alpha = 0$. In Figure 6 the initial sliding zones are symmetric with respect to both coordinate axes. Two examples in Figure 7 show the initial sliding zones for the case when the directions of the weak plane do not coincide with the directions of principal *in situ* stresses. In this case the initial sliding zones are antisymmetric. Restriction (8) is satisfied for any cohesion in the symmetric case and only for the ones shown in Figure 7 in the antisymmetric case.

Characterization of the size of the initial sliding zone can be made by calculating its area, S_{zone}. Since for certain sets of parameters (e.g. $\rho = 0^\circ$, $\tau_c = 0$, $p = 0$, Figure 6) the domain can be unbounded, it is necessary to calculate the area inside any bounded region, for instance, inside the ring $1 \leqslant P \leqslant 3$. Using the step-function ($H(x) = 0$ if $x < 0$, $H(x) = 1$, otherwise), the area of the initial sliding zone (normalized to the area of unit disk) can be easily presented as

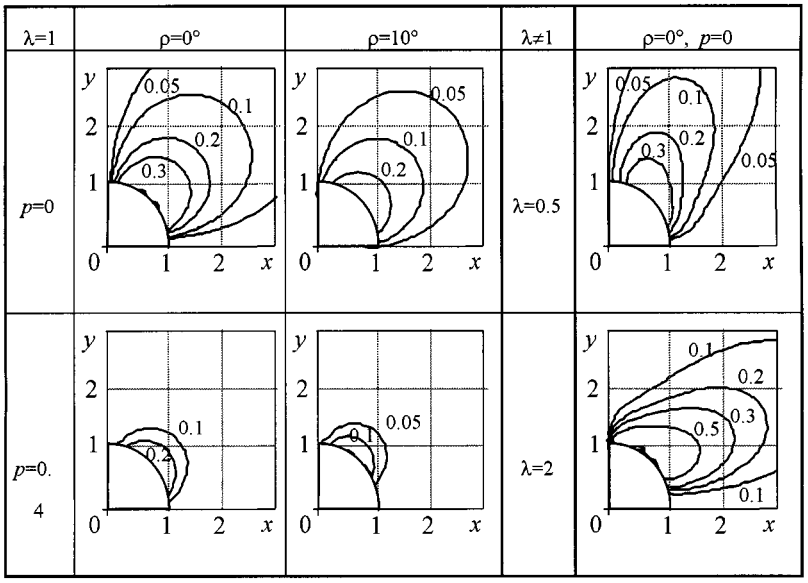

Figure 6. Initial sliding zones for the discontinuity inclination $\alpha = 0°$. Influence of the normalized internal pressure, $p = 0$, 0·4, the friction angle $\rho = 0°$, 10° and the *in situ* stress ratio $\lambda = 0{\cdot}5$, 1, 2

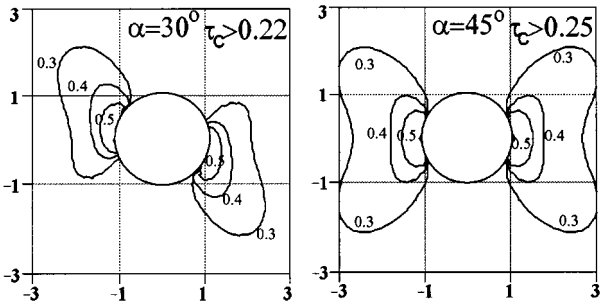

Figure 7. Influence of the discontinuity inclination, α, on initial sliding zones, $\rho = 20°$, $p = 0$, $\lambda = 1$

the double integral in the polar coordinate system (P, θ)

$$S_{\text{zone}} = \frac{1}{2\pi} \int_1^3 P \, \mathrm{d}P \int_0^{\pi} H[F - \tau_c^{\min} H(\tau_c^{\min})] \, \mathrm{d}\theta \tag{21}$$

where the second term in the integrand reflects restriction (8).

After integrating, the area becomes a four-parametric function, $S_{\text{zone}} = S_{\text{zone}}(\alpha, \lambda, p, \rho)$. Dependencies $S_{\text{zone}}(\alpha, \lambda, p, \rho)$ versus α are shown in the Figure 8(a) for different parameters λ, p, ρ. The same dependencies for a specific value of the normalised cohesion $\tau_c^{\min} = 0{\cdot}25$, are shown in Figure 8(b).

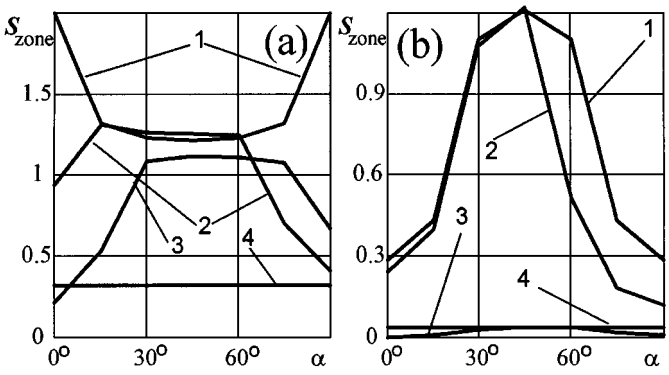

Figure 8. Normalized areas of the initial sliding zones versus angle α, (a) corresponds to $\tau_c^{min} = \tau_c^{min}(\alpha, \lambda, \rho)$, (b) corresponds to $\tau_c^{min} = 0{\cdot}25$: (1) $\lambda = 0{\cdot}5$, $\rho = 0^\circ$, $p = 0$; (2) $\lambda = 2$, $\rho = 10^\circ$, $p = 0{\cdot}4$; (3) $\lambda = 0{\cdot}5$, $\rho = 10^\circ$, $p = 0{\cdot}4$; (4) $\lambda = 1$, $\rho = 10^\circ$, $p = 0{\cdot}4$

One can see the difference: while all curves in the right-hand side plot reach maxima at the point $\alpha = 45^\circ$, the curves in the left-hand side plot may have no maximum at all. This is explained by the fact that the chosen value of $\tau_c^{min} = 0{\cdot}25$ in the right-hand side plot is always greater than the calculated values of $\tau_c^{min}(\alpha, \lambda, \rho)$ in the left-hand side plot. Hence a number of domains situated as a whole within the considered ring $1 \leqslant P \leqslant 3$ in the first case is less than in the second case. If the external radius of the ring increases the curves in the both plots will have the same qualitative behaviour.

4. PROPAGATION OF SLIDING

In this section a model of the borehole instability in a rockmass with a set of parallel joints (Figure 9(a)) and a model of rockburst associated with slip on a discontinuity situated near a longwall excavation (Figure 9(b)) will be discussed. Both models assume that sliding over these discontinuities can be modelled by propagation of the shear crack over the plane of weakness in an elastic rockmass, and is correspondingly described by the solution of the mathematical problem formulated in Section 2.

4.1. Assumptions in modelling

The application of the considered mathematical problem to the description of real rupture processes of the rock mass has some limitations. First of all, the positions of the excavation and the discontinuity have to satisfy the plane-strain conditions. Even if the discontinuity is parallel to the excavation axis these conditions can only be satisfied at a certain distance from the excavation face.

Moreover, it is necessary to assume that significant fracture along the discontinuity could not happen due to the influence of the excavation face. Otherwise the stress field caused by the advance of the excavation will be different from the stress state examined above. This means that either the resistance to shear over the discontinuity should be sufficient to prevent sliding or the discontinuity should be situated such that sliding is not possible under the stress state

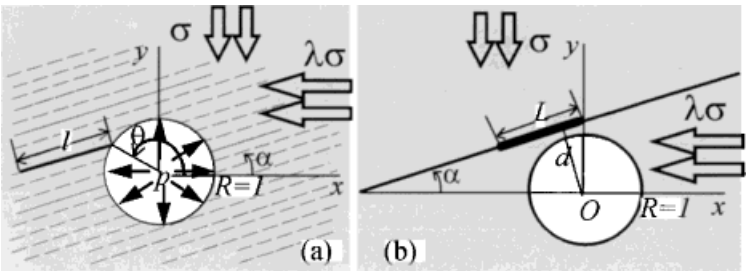

Figure 9. Borehole in jointed rocks (a), slip on a discontinuity situated near excavation (b)

near the face of the excavation. A high level of the internal pressure also reduces the probability of sliding since it decreases the stress concentration.

For simplicity an extra assumption is also required. The profile of the effective shear stresses (function F, see expression (9)) along the weak plane has two or more peaks, which means that cohesion is to be considered high enough to prevent the simultaneous appearance of a second sliding zone on the discontinuity. On the other hand, it should be less than the peak to ensure the possibility of sliding. There are two equal peaks in symmetrical cases $\alpha = 0^\circ$ or $\alpha = 90^\circ$, hence two sliding zones may develop simultaneously on the discontinuity in this ideal situation. These cases have been analysed earlier[21]. Here the case of a single sliding zone modelled as a shear crack is considered. As a simplification the cohesion is assumed to be 80 per cent of the maximum effective shear stresses, $\tau_c = 0{\cdot}8\tau_c^{\max}(d, \alpha, \lambda, p, \rho)$.

4.2. Propagation of sliding from the borehole in jointed rocks

Numerous 2-D models describing the behaviour of jointed rocks with boreholes have been developed recently (for details see, for instance, Reference 8 and references cited there). It is assumed in this study that the internal pressure in the borehole provides elastic deformation of the rockmass during borehole drilling. Then, after the internal pressure drops, sliding may occur along one or a certain number of joints producing irreversible deformation, Figure 9(a). This process may be considered as an initial phase of breakout.

Suppose the density of joints is sufficiently high to intersect equi-probably the boundary of the borehole at any point. The sliding will start at the point at the borehole boundary where the effective shear stress has a maximum (see Figures 4 and 5, Section 3). This point is specified by the angle θ, Figure 9(a). The angle θ is approximately equal to $\alpha + 45^\circ + \rho/2$ ($\lambda > 1$) for all parameters α, ρ, p from the considered range of their variation.[21] Using this value the corresponding value of parameter d can easily be calculated, $d = \cos(45^\circ - \rho/2)$. One of the ends of the edge shear crack which models sliding also becomes known, so that $b = b_0 = -\sin(45^\circ - \rho/2)$ if $\lambda < 1$ or $a = a_0 = -\sin(45^\circ - \rho/2)$ if $\lambda > 1$. The position of the other end is determined from the solution of equation (5) under condition (11).

After all simplifications, four parameters α, λ, p, ρ affect the length of sliding, which is calculated as a balanced length of the shear crack $l = l(\alpha, \lambda, p, \rho) = b(\alpha, \lambda, p, \rho) - a(\alpha, \lambda, p, \rho)$. The following sets of parameters have been used in numerical calculations: $\alpha = 0^\circ, 15^\circ, \ldots, 90^\circ$; $\lambda = 0{\cdot}5, 1, 2$; $p = 0, 0{\cdot}4, 0{\cdot}6$; $\rho = 0^\circ, 10^\circ, 20^\circ$. The results are presented in Figure 10, as funtions of normalized lengths of slidng, l, versus joint inclinations, α. In comparison with the initial length,

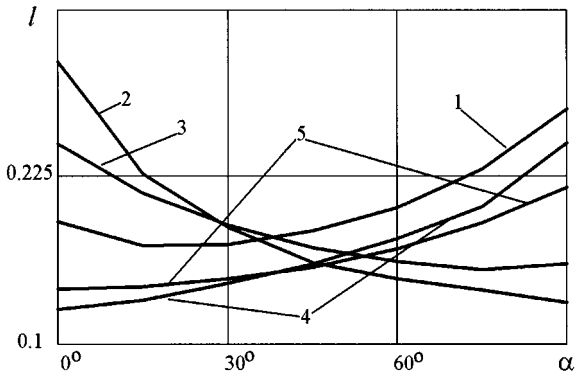

Figure 10. Normalized length of the sliding zone, l, versus joint inclination, α. 1—$\lambda = 2$, $p = 0$, $\rho = 0°$; 2—$\lambda = 0{\cdot}5$, $p = 0$, $\rho = 0°$; 3—$\lambda = 0{\cdot}5$, $p = 0$, $\rho = 10°$; 4–$\lambda = 0{\cdot}5$, $p = 0{\cdot}4$, $\rho = 10°$; 5—$\lambda = 2$, $p = 0$, $\rho = 20°$

l_0, $l_0(\alpha, \lambda, p, \rho) = b_0(\alpha, \lambda, p, \rho) - a_0(\alpha, \lambda, p, \rho)$, obtained from the elastic solution (Section 3.4), the length of sliding obtained here becomes 1.7–2.6 times more.

The obtained lengths of sliding zones are the maximum possible values since the mode II fracture toughness has been assumed zero ($K_{\mathrm{IIc}} = 0$). As a result of this assumption the stresses at the crack tip becomes bounded, and cannot strongly affect the elastic stress field. Hence, if the distance between joints is greater than a typical width of a zone where the influence of the shear crack is high, then new (parallel) cracks cannot appear due to the influence of the first crack. Otherwise formation of such cracks will be possible and appearance of these new cracks may be considered as a mechanism of breakout.

It should be noted that the obtained values of lengths of sliding zones do not exceed the borehole radius ($l < 1$), which is a consequence of the assumption that the normalized cohesion, τ_c, is 80 per cent of the maximum effective shear stresses, $\tau_c^{\max}$. For low values of τ_c the length of sliding increases, however, the ratio l/l_0 weakly depends on this parameter. For example, for $\alpha = 45°$, $\lambda = 0{\cdot}5$, $p = 0$, $\rho = 10°$, this ratio is $l/l_0 = 1{\cdot}65$ *for* $\tau_c = 0{\cdot}8\tau_c^{\max}$ and $l/l_0 = 1{\cdot}93$ for $\tau_c = 0{\cdot}5\tau_c^{\max}$.

4.3. Sliding propagation over a discontinuity situated near a circular opening

Sliding-induced microseismicity is often observed in excavations situated near discontinuities (see, for instance, data from microseismic monitoring[22]). Since rockbursts are associated with a violent release of energy,[7] unstable propagation of sliding over the discontinuity may produce a rockburst. If rockburst has occurred, the release of energy would be proportional to the size of sliding, i.e. the length, L, in Figure 9(b). To estimate the maximum length of sliding it is necessary to consider all available positions of the balanced shear crack neglecting the fracture toughness over the discontinuity (condition (11) for both ends of shear crack).

In contrast to the previous case, where the parameter d has been found, this parameter can vary over a wide range. If the discontinuity intersects the opening the results will be qualitatively similar to those presented above. Therefore, only the case of non-intersection is analysed here. Furthermore, if the distance increases then the influence of the opening becomes less, so it is necessary to set up an upper bound for the parameter d. It is assumed that the range $1 < d < 2$ for distance d is applicable for all calculations.

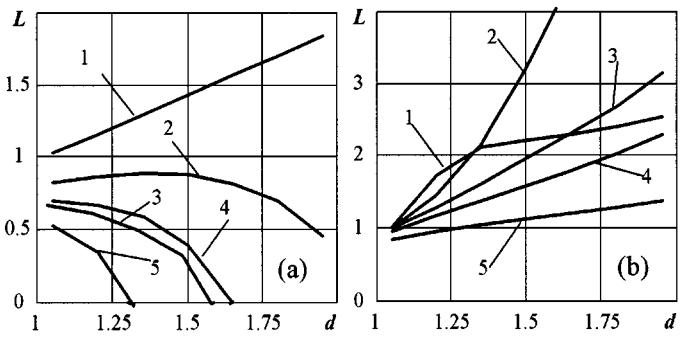

Figure 11. Normalized length of sliding part, L, of the fault versus normalized distance, d. (a) Hydrostatic *in situ* stresses: 1—$p = 0, 0{\cdot}4, 0{\cdot}6$, $\rho = 0^\circ$; 2—p = 0, $\rho = 10^\circ$; 3—$p = 0$, $\rho = 20^\circ$; 4—$p = 0{\cdot}4$, $\rho = 10^\circ$; 5—$p = 0{\cdot}4$, $\rho = 20^\circ$. (b) Non-uniform *in situ* stresses $\lambda = 2$: 1—$\alpha = 0^\circ$; 2—$\alpha = 30^\circ$; 3—$\alpha = 45^\circ$; 4—$\alpha = 90^\circ$; 5—$\alpha = 90^\circ$

The length of sliding, L, has been found as the length of the balanced shear crack (condition (11)), $L = L(d, \alpha, \lambda, p, \rho) = b(d, \alpha, \lambda, p, \rho) - a(d, \alpha, \lambda, p, \rho)$. The results of the calculations are shown in Figure 11. The case of hydrostatic *in situ* stresses ($\lambda = 1$) is presented in Figure 11(a) for $p = 0$, 0·4, 0·6, $\rho = 0^\circ$, 10°, 20°. When $\rho = 0^\circ$, the length of the crack does not depend on p which is explained by the chosen value of $\tau_c = 0{\cdot}8\tau_{\max}(d, 0, 1, p, \rho)$. In this case, the length increases proportionally to d (line 1). As one can see an increase in the internal pressure or/and the friction angle (curves 2–5) reduces the length of the sliding part. The influence of the discontinuity inclination and non-uniformity of *in situ* stresses on the length is illustrated in Figure 11(b) for the special case of $p = 0$, $\rho = 0^\circ$, $\lambda = 2$. The maximum length is reached for the fault inclined at 30° to the direction of the major principal *in situ* stress. The magnitude of the length increases when the distance increases, which is also explained by the chosen value for the normalized cohesion $\tau_c = 0{\cdot}8\tau_{\max}(d, \alpha, 2, 0, 0)$.

When the sliding on the discontinuity stops, a new stress state is created to provide equilibrium. To evaluate the new stresses, it is necessary to substitute the obtained solution for the derivative of the jump of tangential displacements over the crack in the expression for complex potentials (4). After integrating, the stress tensor can be calculated at any given point, in particular, at the crack contour where the tangential stress component may be positive. This happens if the absolute value of the additional tensile stresses in the direction of the discontinuity exceeds the compressive stresses acting in the same direction prior to sliding. If the total stress has reached the tensile strength of rock it would produce a tensile crack. If such a crack would propagate dynamically in the direction of the opening it might produce a new rockburst.

The additional tangential stress on the sliding part of the fault has a jump proportional to the density of the jump of tangential displacements. The expression for these stresses has the form

$$\sigma_r^{\pm}(z) = 4\mathrm{Re}(\Phi_2^{\pm}(z)) - \sigma_n(z), \qquad \Phi_2^{\pm}(z) = \frac{\pm 1}{2}\mu(t) + \frac{1}{2\pi \mathrm{i}}\int_a^b \Phi^*(z, t(r))\mu(t)\,\mathrm{d}r \tag{22}$$

where the normal component of the stresses, σ_n, is continuous and may be calculated directly by applying Kolosov's formulae, while the boundary value of the potential $\Phi(z)$ is presented as a sum of the solution $\mu(t)$ and the singular integral in accordance with the Sokhotski formulae.[21]

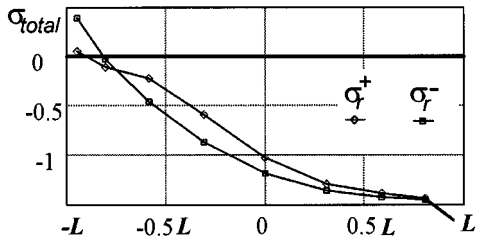

Figure 12. Profile of the total tangential stress over sliding part of the discontinuity

Calculations for different positions of the fault and different sets of parameters show that the additional stresses σ_r are always less than the initial stresses. Hence the appearance of the tensile total stresses is not possible when the mode II fracture toughness over the fault is zero. However, if the mode II fracture toughness is not negligible, then the stress field is singular at both ends, which explains the appearance of tensile stresses. An example given below illustrates this fact.

Let the *in situ* stress ratio be $\lambda = 2$, the fault inclination be $\alpha = 90^\circ$, the distance be $d = 1{\cdot}05$, the coordinates of the ends be $a = 0{\cdot}17$, $b = 1{\cdot}48$, the normalized cohesion be $\tau_c = 0{\cdot}22$, and the friction angle be $\rho = 0^\circ$. For this case the normalized SIFs for both ends are equal to $K_{II} = 0{\cdot}11$. If the fracture toughness is $K_{IIc} = 0{\cdot}11\ (1{\cdot}31R\pi)^{1/2}\sigma$, the crack will be in equilibrium. The total tangential stresses at the crack boundaries calculated at Chebyshev's points are shown in the Figure 12. Zones of tensile stresses exist for both boundaries of the crack close to the crack end located near the opening.

4.4. Comparison of direct and iterative methods

Recently, in connection with developing the models of behaviour of the discontinuity near the borehole, geometrically similar problems have been considered by using an approximate method[9] which does not take into account the back influence of the borehole onto the crack propagating over the discontinuity. In the case when the discontinuity does not intersect the borehole this method corresponds to neglecting the integral term in (18) and correspondingly to accounting of the only first term in the iterative procedure (19). The accuracy of this method can easily be estimated by comparing results with those obtained by the direct method. In addition, it is possible to find out (at least for the case considered in this study) the number of iterations which are required to reach the correct results.

For this purpose it is possible to simplify the problem as follows. Since the right-hand side of the singular integral equation (5) is expressed as a linear combination of seven functions: 1, $\mathrm{Re}(\zeta^{-i})$, $\mathrm{Im}(\zeta^{-j})$, $(\zeta = r + id)$, $j = 2, 3, 4$, the solution of the equation can be obtained for each function separately. Moreover, the kernel of the equation does not depend on the angle α, and weakly depends on the friction angle ρ. Hence one can consider the one-parameter problem, assuming $\rho = 0$ and using the initial values of a_0, b_0 from any considered examples (for instance the case of $\lambda = 1$) as coordinates of the cracks ends.

The results of calculation of the SIFs for the left and right ends of the shear crack are listed in the Table I. The SIFs were calculated by both the direct method and by the iterative method. The initial value (0-iter) in the iterative method corresponds to accounting only the right-hand side (without the regular part of the kernel). The first iteration (1-iter) takes into account the stresses

Table I. Stress intensity factors and relative errors

Distance	Function	Left (remote) end							Right end						
		1	$\mathrm{Re}(\zeta^{-2})$	$\mathrm{Re}(\zeta^{-3})$	$\mathrm{Re}(\zeta^{-4})$	$\mathrm{Im}(\zeta^{-2})$	$\mathrm{Im}(\zeta^{-3})$	$\mathrm{Im}(\zeta^{-4})$	1	$\mathrm{Re}(\zeta^{-2})$	$\mathrm{Re}(\zeta^{-3})$	$\mathrm{Re}(\zeta^{-4})$	$\mathrm{Im}(\zeta^{-2})$	$\mathrm{Im}(\zeta^{-3})$	$\mathrm{Im}(\zeta^{-4})$
d															
1·05	SIF	− 1·13	0·413	− 0·291	− 0·002	− 0·38	− 0·138	0·151	− 1·142	0·395	0·299	− 0·003	0·399	− 0·125	− 0·157
Relative	0-iter	0·11	0·17	0·19	15·0	0·16	0·29	0·26	0·12	0·19	0·22	9·8	0·18	0·34	0·32
error for	1-iter	0·02	0·04	0·04	5·7	0·04	0·09	0·07	0·03	0·05	0·06	3·9	0·04	0·11	0·09
1·2	Exact	− 1·034	0·289	− 0·18	0·006	− 0·266	− 0·081	0·08	− 1·04	0·258	0·176	0·009	0·277	− 0·06	− 0·077
Relative	0-iter	0·03	0·04	0·09	− 0·5	0·08	0·07	0·11	0·04	0·05	0·1	− 0·35	0·08	0·09	0·15
error for	1-iter	0	0	0·01	− 0·12	0·01	0·01	0·01	0	0	0·01	− 0·09	0·01	0·01	0·02
1·35	Exact	− 1·012	0·23	− 0·124	0·005	− 0·202	− 0·058	0·051	− 1·018	0·196	0·121	0·009	0·216	− 0·038	− 0·047
Relative	0-iter	0·01	0·01	0·06	0·16	0·05	− 0·01	0·07	0·02	0·01	0·06	0·08	0·05	− 0·01	0·1
error for	1-iter	0	0	0	0·01	0	0	0	0	0	0·01	0	0	0	0·01
1·5	Exact	− 1·005	0·173	− 0·087	0·005	− 0·163	− 0·035	0·03	− 1·009	0·157	0·084	0·006	0·168	− 0·027	− 0·029
Relative	0-iter	0	0	0·05	0·18	0·04	− 0·03	0·07	0·01	0	0·05	0·15	0·04	− 0·04	0·08
error for	1-iter	0	0	0	0·01	0	0	0	0	0	0	0·01	0	0	0·01

reflected from the hole boundary. Relative errors for initial and first iterations are shown under the corresponding values for the SIFs calculated by the direct method. One can see that both errors are rapidly decreasing functions of the distance. Even for a small distance $d = 1{\cdot}05$, the first iteration gives relative errors within 1–11 per cent, except the case of ζ^{-4} where big errors are caused by very small magnitude of SIF. For distances $d > 1{\cdot}2$, it is possible to neglect the back influence of the opening and take into account only stresses which could be created by the opening in intact rock at the place of the discontinuity. In this case the error is less than 10 per cent (except the case of ζ^{-4}), which is related to the accuracy of the direct method with (approximately) 8–10 nodes (10 nodes have been used in these calculations). In comparison with the range of the strength variation in real rocks, this accuracy seems to be more sufficient.

5. CONCLUSIONS

The numerical solution for the problem of propagation of a shear crack near a circular hole has been obtained. The results are used to model rock failure due to developing the sliding zone over a part of the discontinuity situated near an excavation.

The initial phase of borehole breakout has been modelled as propagation of sliding from the wall of the borehole along a single joint. In this case, the position of the point where sliding starts mainly depends on the inclination of the joints with respect to the principal *in situ* stresses. If the cohesion is assumed to be 80 per cent of the maximum shear stresses, the maximum length of sliding will be 1·7–2·6 times greater than that calculated from the elastic solution.

It is shown that rockburst may be associated with unstable propagation of sliding over a part of discontinuity if this process is accompanied by a violent release of energy. The length of the sliding part over the discontinuity has been calculated for the different positions of the discontinuity, and different values of the load and strength parameters involved in the problem. In particular, it has been shown that increasing the internal pressure (due to support reaction) reduces the length of the sliding part, which may be considered as a method of prevention of rockbursts. The influence of the discontinuity inclination and non-uniformity of *in situ* stresses on the sliding length is mostly significant.

It has been found that increasing fracture toughness K_{IIc} can induce tensile tangential stresses on the sliding part of the discontinuity. If these stresses exceed the tensile strength of rock, a new fracture can emanate from the discontinuity and propagate towards the opening, which may eventually lead to rockbursts.

Applicability of the approximate method which does not take into account the back influence of the shear crack on the hole is justified for the case of non-intersection.

ACKNOWLEDGEMENTS

The author is grateful to Dr. A. V. Dyskin and Dr. D. Adhikary for helpful advice and discussion of the results.

NOMENCLATURE

a_0, b_0	initial coordinates of the crack ends
a, b	final coordinates of the crack ends
l_0	initial length of the crack

d	distance between the crack (discontinuity) and the centre of the hole
$F(\xi)$ and $F(r, d, \alpha, \lambda, p, \rho)$	effective shear stresses over the discontinuity
$F_{\max}(\xi)$	maximum effective shear stresses over the discontinuity
G	shear modulus
$G(\eta, \xi)$	regular part of the kernel of SIE (5)
$H(x)$	step-function
$K_{\mathrm{II}}, K_{\mathrm{II}}^{\mathrm{l}}, K_{\mathrm{II}}^{r}$	stress intensity factor of mode II, superindex l/r stands for left/right tip
K_{IIc}	fracture toughness of mode II
$\mathbf{L}$	contour of the shear crack
l	length of the shear crack
L	length of the sliding part of discontinuity
p	internal pressure acting in the hole
R	radius of the hole
S_{zone}	normalised area of the initial sliding zone
$u_n u_\alpha$	is the normal and tangential displacements at the crack, respectively
$[u_\alpha]$	jump of tangential displacements across the crack contour
z	complex coordinate of a point in the plane
α	angle of the crack (discontinuity) inclination
γ	contour of the hole
$\Phi(z)$ and $\Psi(z)$	complex potentials
λ	*in situ* stress ratio (horizontal/vertical)
$\mu(n)$	unknown function proportional to the derivative of the jump in tangential displacements across the crack contour
ν	Poisson's ratio
ρ	friction angle along the crack
σ	vertical *in situ* stress
τ_{c}	cohesion along the crack
$\tau_{\mathrm{c}}^{\max}$	maximum value of cohesion determined as the supremum of the function F
$\tau_{\mathrm{c}}^{\min}$	minimum value of cohesion determined from inequality (8)

REFERENCES

1. O. L. Bowie, 'Analysis of an infinite plate containing radial cracks at the boundary of an internal circular hole', *J. Math. Phys.*, **35,** 60–71 (1956).
2. P. M. Vitvitskii and M. Ja. Leonov, 'Extension beyond the yield point of a plate with a circular opening', *J. Appl. Math. Tech. Phys.*, **4**(1)**,** 109–117 (1962).
3. Y. Murakami (ed.), *Stress Intensity Factor Handbook*, 1, Pergamon Press, Oxford, 1987.
4. H. Tada, P. C. Parisand and G. R. Irwin, *The Stress Analysis of Cracks Handbook*, Paris Production, Inc. (and Del. Research Corporation), St. Louis, Missouri, 1985.
5. Savruk, *Two-dimensional Problems of Elasticity for Body with Cracks*, Naukova Dumka, Kiev, 1981.
6. Erdogan and G. D. Gupta, 'On the numerical solution of singular integral equations', *Quart, J. Appl. Math.*, **30,** 525–534 (1972).
7. B. H. G. Brady and E. T. Brown, *Rock Mechanics for Underground Mining*, George Allen and Unwin, London, 1985.
8. B. Amadei, 'Importance of anisotropy when estimating and measuring *in situ* stresses in rock', *Int. J. Rock Mech. Min. Sci. Geomech. Abstr.*, **33,** 293–325 (1996).
9. M. Triereling and C. Atkinson, 'Pressurisation of a fractured wellbore', *Proc. 2nd North American Rock Mechanics Symp.*, Vol. 2, Montreal, Canada, 1105–1112 (1996).
10. N. I. Muskhelishvili, *Some Basic Problems of the Mathematical Theory of Elasticity*, Noordhoff, Groningem, 1953.

11. R. V. Duduchava, 'Integral equations of convolution type with discontinues pseudosymbols, singular integral equations with fixed singularities and their application to mechanical problems', *Proc. Tiflis Math. Institute AN GSSR*, **60,** 3–135 (1979).
12. Y. S. Ufliand, *Integral Transforms in the Theory of Elasticity*, Nauka, Moscow, 1967.
13. A. N. Galybin, A. V. Dyskin and A. M. Korsunsky, 'An investigation into the stress-field singularity at the mouth of a surface-breaking crack', *Int. J. Solids Struct.*, **29,** 271–277 (1992).
14. A. N. Galybin, 'The growth of a crack from the boundary of a narrow cavity in a biaxially compressed body', *J. Appl. Math. Mech.*, **59,** 467–474 (1995).
15. N. I. Ioakimidis and P. S. Theocaris, 'A comparison between the direct and the classical numerical methods for the solution of Cauchy type singular integral equations', *SIAM J. Numer. Anal.*, **17,** 115–118 (1980).
16. P. S. Theocaris and N. I. Ioakimidis, 'Numerical integration methods for the solution of singular integral equations', *Quart. J. Appl. Math.*, **35,** 173–183 (1977).
17. G. P. Cherepanov, 'Equilibrium of a slope with a tectonic crack', *J. Appl. Math. Mech.*, **40,** 119–133 (1976).
18. E. T. Brown and E. Hoek, 'Trends in relationships between measured *in situ* stresses and depth', *Int. J. Rock Mech. Min. Sci.*, **15,** 211–215 (1978).
19. R. E. Goodman, *Introduction to Rock Mechanics*, 2nd ed., Wiley, New York, 1989.
20. F. D. Gakhov, *Boundary Value Problems*, Dover, New York, 1990.
21. A. N. Galybin and A. N. Mokhel, 'Borehole breakout in rocks with strength anisotropy', *The 1st Australian Congr. on Applied Mechanics 21–23 February 1996*, The Institution of Engineers, Australia Preprint of Papers, 1996, pp. 943–948.
22. P. A. Micula and R. F. Poplawski, 'The seismic monitoring decision at Mt Charlotte Gold Mine', *Proc. Underground Operators Conf.*, Kalgoorlie, Australia, 1995, pp. 79–85.

